Physical Phenomena of Char–Slag Transition in Pulverized Coal Gasification

Suhui Li,* Kevin J. Whitty

Institute for Clean and Secure Energy, University of Utah, 50 South Central Campus Drive,

MEB Room 3290, Salt Lake City, Utah 84112, United States

UU IR Author Manuscript

* Corresponding author. Email: leesuhui@msn.com. Telephone: +1-801-585-9388. Fax: +1-801-585-9291

Abstract

Performance of entrained-flow coal gasifiers is in large part dictated by the burnout behavior of coal particles. In particular, the transition from porous, reactive char to molten, low reactive slag affects overall coal conversion. In this work, the physical phenomena associated with char–slag transition were studied for three coals using a laminar entrained-flow reactor under simulated gasification conditions. Partially oxidized particles with various conversions were prepared at temperatures above the ash fluid temperatures. The physical properties of the char and slag particles were characterized, including the particle density, size, internal surface area and morphology. Results show that at a coal-dependent critical conversion, the particles undergo remarkable physical changes, such as density increase, size reduction and surface area decrease. These phenomena indicate the char–slag transition.

Keywords: porous char; molten slag; ash particle; entrained-flow reactor; coal gasification

1. Introduction

Modern slagging entrained-flow coal gasifiers are operated at high temperatures, typically in the range of 1300–1500 °C [1]. The high operation temperatures help achieve high conversion and break down the tars in the syngas, but create ash melting related issues. For example, during the late stage of gasification, the transition from porous char to molten slag affects coal conversion by changing the burnout behavior of the material. Lin et al. [2] observed an unusual reduction in the reaction rate when gasifying coal chars at conversions above 50% and around ash melting temperature. The phenomenon was attributed to the pore plugging by molten ash, which causes the decrease of the surface area available for gasification. In addition, when the char transforms into slag, its pore structure and morphology undergo significant changes, which

inevitably affect the pore diffusion and thus the gasification of unconverted carbon in the particle [3, 4]. In practical operation of entrained-flow coal gasifiers, it is common to have a considerable fraction (in the range of 30–40%) of carbon remaining in the fine slag [5, 6], which limits carbon conversions to less than roughly 97%. To improve efficiency in the integrated-gasification combined cycle (IGCC) power plants, coal conversions of 99% or higher are desired. Therefore, understanding the physical properties changes associated with the char–slag transition has special technological significance for the practical operation of entrained-flow coal gasifiers.

As coal particles reach high conversions, the stickiness (the intrinsic propensity to stick on the gasifier wall upon striking) of the particle in the char–slag transition stage increases greatly [7, 8]. Computational fluid dynamics (CFD) modeling of entrained-flow gasifiers indicate that a large portion of char and slag particles strike the gasifier wall at different conversions [9–11]. The residence times and burnout behaviors of such particles are presumed to change accordingly upon adhering on the gasifier wall. Indeed, the influence of char and slag particle deposition on carbon burnout has received increasing attention [12–14]. Furthermore, deposition of char and slag particles on gasifier wall contributes to the formation of slag flow, which results in erosion and corrosion of the refractory [15]. Thus, determining the particle fates (sticking or rebounding) upon impacting the gasifier wall facilitates CFD modeling of entrained-flow gasifiers in tracking the particle burnout behavior and deposition behavior. Predicting the char–slag transition is a prerequisite for accurately determining the particle fates.

Despite the extensive research on char gasification and ash formation, the specific nature of the char–slag transition is far from being well understood. Little attention has been paid to characterizing the physical phenomena (changes in particle density, size, internal surface area and morphology) associated with the char–slag transition, particularly at high temperatures and

high conversions in a gasifying environment. In light of the lack of such data, the char–slag transition of three coals was studied using a lab-scale laminar entrained-flow reactor (LEFR). This paper presents the experimental results of the study and the development of an empirical model for predicting the char–slag transition.

2. Material and methods

2.1. Coal sample

Coal rank plays an important role in the reaction behavior during gasification process. Three pulverized coals of different ranks were used for the experiments: Pittsburgh #8 (PT8), Illinois #6 (IL6) and Black Thunder from Powder River Basin (PRB). The PT8 is a high-volatile A bituminous coal, the IL6 is a high-volatile C bituminous coal, and the PRB is a subbituminous coal. All the coals were sieved to a size range of 43–63 μm to minimize the effect of particle size distribution on char burnout. Before sieving, coal samples were dried in a muffle furnace at 104 °C for 24 hours to remove the moisture according to an ASTM method [16]. The properties of the coals and the ashes were determined by Wyoming Analytical Laboratories. The proximate and ultimate analyses and the ash fusion temperatures are listed in Tables 1 and 2, respectively.

2.2. Experimental apparatus and procedure

Char and slag particles were prepared using a lab-scale LEFR under gasification conditions. A schematic diagram of the LEFR is shown in Fig. 1. It consists of a high temperature furnace (Carbolite, single zone, 1600 °C maximum operation temperature and 610 mm heated length), a coal feeder, a sample collector, gas supply and a cooling water circulator. Two co-axial alumina tubes (89 mm o.d. × 75 mm i.d. × 1500 mm long and 57mm o.d. × 50 mm i.d. × 1000 mm long, respectively) are installed vertically inside the furnace. The inner tube is used as the reactor. The reaction gas (a premixed air–nitrogen mixture) is injected through three injection ports on the

bottom flange and is preheated when it flowed upwards through the annulus between the two co-axial tubes. When the reaction gas reaches the top of the annulus, it makes a 180 ° turn and flows down into the inner tube through an alumina honeycomb flow straightener. The flow straightener has a sufficient pressure drop to generate a uniform and laminar flow to ensure the entrained particles travel along the centerline of the reactor tube experiencing identical reaction conditions. Coal particles are fed into the reactor through an injection probe using a vibrating syringe pump type coal feeder with nitrogen as carrier gas. The injection probe is water-cooled to prevent coal particles from being pyrolyzed before reaching the reaction zone. Upon injection into the reactor, the coal particles react with the reaction gas to produce char and ash particles. Conversions of the char and ash particles are controlled by adjusting the residence time of the particles in the reactor. After undergoing partial conversion, resulting particles exit the reactor and are collected in a cyclone via a collection probe. Nitrogen is injected into the collection probe through a sintered stainless steel tube to quench the product stream and reduce the thermophoresis deposit of the char particles on the cold surface of the probe. The cut diameter of the cyclone is about 2–4 μm.

2.3. Experimental conditions

The pressure inside the reactor was maintained at ambient pressure, 0.85 bar (the altitude of Salt Lake City is about 1350 m). The furnace temperature was set to 1500 ºC for the PT8 coal and 1400 ºC for the IL6 and PRB coal, which are above the ash fluid temperatures of the specific coal ashes. The feeding rate of coal particles was 30 mg/min. The flow rate of air in the reaction gas mixture was varied for different coals to keep a stoichiometric ratio (oxidant/fuel, molar basis) of 0.7, which provided an overall reducing atmosphere in the reactor. The term oxidant is defined as the oxygen contained in the air and coal. The term fuel refers to all the combustible elements (carbon, sulfur and hydrogen) in the coal. The experimental runs for preparing fresh

chars by devolatilization used pure nitrogen. The residence time of coal particles in the reactor was varied from 1 to 6 s in 1 s increment. The use of a long residence time was due to the low oxygen content (0.7%–4.6%) in the reaction gas in accordance with the low feeding rate of coal.

2.4. Sample characterization

Carbon content of the collected char and slag particles was determined using a hot foil loss–on–ignition (LOI) instrument (FERCO, HF400). About 0.01 g of sample was completely burned using this apparatus. The sample was weighed before and after the LOI analysis. The carbon content was calculated by

$$C_{char}^{carbon} = \frac{m_{char} - m_r}{m_{char}} \times 100\% \quad (1)$$

where C_{char}^{carbon} is the weight fraction of residual carbon and other combustible elements (sulfur and hydrogen) in the char and slag particles, m_{char} is the mass of the sample before the LOI analysis and m_r is the mass of the burnout residual (assuming pure ash) after the LOI analysis.

Coal conversion of the char and slag particles was determined with an established method [17, 18]. This method uses ash as a tie component (tracer) to calculate the coal conversion X by

$$X = \left(1 - \frac{C_{char}^{carbon} C_{coal}^{ash}}{(1 - C_{char}^{carbon}) C_{coal}^{carbon}}\right) \times 100\% \quad (2)$$

where C_{coal}^{ash} is the weight fraction (moisture free) of ash in the parent coal, and C_{coal}^{carbon} is the weight fraction (moisture free) of carbon and other combustible elements (sulfur and hydrogen) in the parent coal. C_{char}^{carbon} was determined by the LOI analysis using eq 1. C_{coal}^{ash} was determined by the proximate analysis presented in Table 1. C_{coal}^{carbon} was determined by subtracting the sum of coal ash content (moisture free) and coal oxygen content (moisture free) from 100%. The coal oxygen content can be calculated from the ultimate analysis in Table 1. Borrego and Alvarez [18] discussed the error of calculating the coal conversion using ash tracer method qualitatively. They

concluded that the ash tracer method is acceptable for mainly comparative purposes between experiments performed at a single temperature varying only the reaction atmosphere.

The apparent (bulk) density of the char and slag particles was measured with the method used by Tsai and Scaroni [17]. In brief, a graduated cylinder was filled with the sample and then tapped gently for uniformly packing to the minimum volume. The mass of the cylinder was measured before and after being filled with particles. Assuming the same packing factor, the bulk density of the particles ρ_a was calculated as

$$\rho_a = \frac{m_{cp} - m_c}{V} \quad (3)$$

where m_{cp} is the mass of the filled cylinder, m_c is the mass of the empty cylinder and V is the volume that the particles occupy in the cylinder (including the interparticle voids). The effective particle density was calculated as

$$\rho_p = \frac{\rho_a}{1-\phi} \quad (4)$$

where ρ_p is the effective particle density and ϕ is the packing voidage, which was assumed to be 0.5 according to previous research [17, 19]. The use of a constant voidage in the calculation of particle density is valid only on conditions that: (1) particles have a narrow size distribution and, (2) particle size does not change greatly versus conversion. In general, the voidage of a packed bed increases with decreasing particle size. The error associated with the use of a constant voidage was estimated to be in the range of 10–20% [17].

The particle size was statistically determined using an Olympus optical microscope and Image J software. Images of a number of particles (20–100) were taken using the microscope. The Image J software automatically locates the individual particles in the images and calculates

the projected area of the individual particles. By assuming the particles are spherical, the mean particle size was determined from the averaged diameter of the examined particles.

Internal surface area of the char and slag particles was measured by isothermal gas adsorption using a surface area and porosimetry analyzer (Micromeritics, Tristar II 3020) with N_2 as adsorptive gas at 77 K (liquid nitrogen bath). Each sample was degassed under 250 °C with a N_2 gas flow for 4 hours to remove the moisture and other adsorbed gases before analysis. The total surface area was obtained by analyzing the isotherms using the Brunauer–Emmett–Teller (BET) method. The micropore surface area was calculated by analyzing the isotherms using t-Plot with Harkins–Jura thickness curve.

Microimages of the char and ash particles were captured using a scanning electron microscope (FEI Nova nano) equipped with an Everhart–Thornley detector under high vacuum mode. The accelerating voltage was 10–15 kV and the working distance was 5 mm. Particles were affixed to the sample holder using carbon tape as conductive base.

3. Results and discussion

3.1. Particle burnout behavior

Conversions of the three coals are presented in Fig. 2 as a function of residence time. Data in Fig. 2 are the averaged values of three experimental runs for each sample. Error bars for the IL6 coal data were calculated using sample standard deviation with a confidence interval of 90%. The error was mainly due to the variation in controlling the flow rate of the reaction gas using rotameters and was partially introduced by determining the carbon content using LOI analysis. As expected, the conversion increased with residence time. At the same residence time, the coal conversion increased as coal rank decreased from PT8 to IL6 and PRB. This is because the lower rank coal has higher reactivity than the higher rank coal.

3.2. Particle density and size

Particle densities of the char and slag samples prepared from the PT8 coal are presented in Fig. 3 as a function of conversion. Particle density of the parent coal is also included in Fig. 3 for comparison.

Up to 85% conversion, the particle density of the partially converted char remained basically constant and slightly lower than that of the pyrolyzed char, suggesting a porous structure similar to that of the pyrolyzed char. Maloney et al. [20] observed that char particle densities remained virtually unchanged with a slight upward trend up to 84% mass loss (comparable to conversion) during the combustion of a subbituminous coal. They attributed this phenomenon to the shrinkage of char particles with conversion, which tends to keep the porous structure. Hurt and colleagues [21, 22] also reported gasification-induced shrinkage up to 85% conversion. They concluded that shrinkage is due to densification of internal microporous structure and it reflects complex changes in internal morphology of the particle. Therefore, the relatively constant particle densities before 85% conversion suggest shrinkage of the char particles.

The particle density of the partially converted char started increasing at about 89% conversion and surpassed that of the pyrolyzed char at about 91% conversion. This suggests that the char particle started transforming into slag at about 89% conversion. Maloney et al. [20] observed an upward trend of particle density with decreasing particle size during char burnout process. Therefore, the increase in particle density in Fig. 3 can be tentatively attributed to the size reduction of char and slag particles as conversion increased. There are two possible mechanisms that contribute to size reduction: shrinkage and fragmentation.

Shrinkage refers to the decrease in external dimensions of a particle while maintaining the integrity of the char particle [23, 24]. Fragmentation is the phenomenon in which a single

particle breaks into more than one piece of smaller particles or fragments [25]. To see which mechanism is responsible for the size reduction during the gasification process of the PT8 coal, the particle size measured by optical microscope was compared with that determined by theoretical calculation. The microscopic measurement, which was described in the experimental section, gives the true particle size. The theoretical calculation is based on the principle that change in particle density is caused by changes in particle mass and volume as well as two assumptions: (1) one parent coal particle forms a single char or slag particle in the burnout process, and (2) the particle is spherical. This method is described as follows.

For a char or slag particle with coal conversion X, its mass m_p can be expressed as

$$m_p = \left(1 - C_{coal}^{carbon} X\right) m_0 \tag{5}$$

where C_{coal}^{carbon} is the parent coal carbon content defined in eq 2 and m_0 is the mass of the parent coal particle. According to the definition of density, the mass of a spherical char or slag particle can be expressed in terms of particle density ρ_p and diameter d_p as

$$m_p = \frac{1}{6}\pi d_p^3 \rho_p \tag{6}$$

and the mass of the parent coal particle can be expressed as

$$m_0 = \frac{1}{6}\pi d_0^3 \rho_0 \tag{7}$$

where d_0 and ρ_0 are the diameter and density of the parent coal particle, respectively. By substituting m_p and m_0 in eq 5 with eqs 6 and 7, the particle size d_p can be calculated as

$$d_p = d_0 \left[\left(1 - C_{coal}^{carbon} X\right) \frac{\rho_0}{\rho_p}\right]^{\frac{1}{3}} \tag{8}$$

where d_0 is known, ρ_p and ρ_0 can be determined using eq 4 and C_{coal}^{carbon} is the moisture free coal carbon content defined in eq 2.

Particle sizes determined using the two methods are presented in Fig. 4 for comparison. Both of the methods indicate decreasing particle size with increasing conversion. However, the measured and calculated particle sizes do differ. Up to about 85% conversion, the measured sizes roughly agree with the calculated values, suggesting that the assumption of one coal particle forming one char particle is valid and the particle size reduction was due to shrinkage. From about 89% conversion, the measured particle sizes (true value) became much smaller than the calculated values, indicating that the assumption of one particle is inappropriate at this point. Fragmentation of the PT8 coal char particles appears to have begun at about 89% conversion, which led to further size reduction.

Particle densities of the char and slag samples prepared from the IL6 and PRB coals are presented in Fig. 5. In general, the evolution of the particle densities of the IL6 and PRB char and slag samples followed the same trend as the PT8 char and slag particles. Data in Fig. 5 suggest that the char–slag transition occurred at about 88% and 92% conversion for the IL6 and PRB coal, respectively.

Particle sizes of the char and slag samples prepared from the IL6 and PRB coals are shown in Fig. 6. The measured (true) particle sizes started dropping below the calculated values at about 91% and 94% conversion for the IL6 and PRB coal, respectively. This phenomenon suggests that fragmentation of the IL6 coal char and PRB char took place at about 91% and 94% conversion, respectively.

On the basis of the analyses on the particle density and size, it can be concluded that shrinkage dominates the particle size reduction during the initial stage in the gasification of the three coals, whereas fragmentation results in more significant size reduction in the later stage (char–slag transition).

3.3. Internal surface area

Bar-Ziv and Kantorovich [26] reviewed the shrinkage and fragmentation behavior of char particles during oxidation. They concluded that: (1) shrinkage occurs in materials with high microporosity and high internal surface area, and (2) fragmentation takes place when macroporosity reaches a threshold value. Therefore, the shrinkage and fragmentation behavior of char particles of the three coals indicate that the internal surface area of chars decreased abruptly upon fragmenting due to loss of microporosity. Examination of the micropore surface areas of the char and slag particles can provide insight into the variation of microporosity.

The total and micropore surface areas of the PT8 coal char and slag particles are plotted in Fig. 7 as a function of conversion. The total surface area increased with conversion in the initial stage of the burnout process and then started decreasing at about 91% conversion. The micropore surface area followed the same trend but decreased at about 89% conversion, agreeing well with the particle fragmentation which occurred at about 89% conversion. Liu et al. [27] attributed the decrease of char surface area at high temperatures to ash melting, which closed the macropores of the char resulting in an inaccessibility of the pores to adsorptive gas. Lin et al. [2] also pointed out that ash melting contributes to the decrease in the surface area of micropores and mesopores, especially at high conversion because the ash content increased with conversion.

The PT8 coal used in this study has an ash fluid temperature of 1229 °C under reducing conditions, which is well below the 1500 °C temperature at which the experiments were conducted. The ash in the char particles presumably was melted at 1500 °C. Therefore, the decrease in the total surface area can be attributed to ash melting in the char. In addition, the consumption of carbon at high conversions resulted in loss of micropores, resulting in the decrease of micropore surface area. The melting of ash and loss of microporosity in the char lead

to a substantial structural change: the transformation from porous char to molten, low-porosity slag. Thus, the decrease of the total surface area at about 91% is an indicator of the char–slag transition.

The total and micropore surface areas of the IL6 and PRB coal char and slag samples started decreasing at about 88% and 92% conversion, respectively, as shown in Figs. 8 and 9. Similar to the PT8 coal, this phenomenon suggests the char–slag transition for the IL6 and PRB coals took place at about 88% and 92% conversion, respectively.

3.4. Particle morphology

Morphological changes during the char–slag transition are revealed by the SEM images of the samples. Such information can be used to confirm the critical conversions at which the transition occurred that were determined on the basis of the changes in particle density, size and internal surface area. Furthermore, the SEM images provide visual observation of the mineral matter transformation, which promotes the understanding of the effect of ash melting on the variation of the particle internal surface area. Mineral matter in pulverized coal that contributes to ash formation is classified in two categories according to the association between minerals and carbon matrix: excluded minerals and included minerals [28, 29]. Excluded minerals are discrete mineral grains that are not associated with coal particles. Included minerals are embedded within or organically bonded with the carbon matrix in coal particles. Therefore, only included minerals are involved in the char–slag transition due to their association with carbon matrix. SEM images of partially converted char and slag particles prepared from the PT8 coal are presented in Fig. 10. Morphological changes and mineral matter transformation during the char–slag transition are interpreted with these SEM images.

At low and medium conversions (Fig. 10a, 10b and 10c), the carbon material in the char was consumed to an extent that shrinkage occurred, as indicated by the particle size data in Figure 4. Upon shrinking, the char surface receded and a few minerals (indicated by the bright droplets) became exposed on the char surface. Most of the minerals, however, were still encapsulated by the carbon matrix because the conversion was not sufficiently high. In this stage, exposure of included minerals on char surface is mainly due to particle shrinkage (surface recession).

As conversion proceeded, there was less carbon remaining in the char and the particle fragmented, as indicated by its size (Fig. 10d). As a consequence, more and more included minerals became exposed on the particle surface. When sufficient minerals were exposed on the particle surface), the char–slag transition started. In this stage, exposure of included minerals on the char surface is mostly caused by fragmentation. A few of the exposed minerals likely remained attached on the particle surface due to the molten ash surface tension [30] and became molten at temperatures above the ash fluid temperature. These molten minerals coalesced when they gradually met each other on the receded particle surface and eventually merged with the molten minerals inside the size-reduced particle (Fig. 10e). When coalescence of the minerals was completed, the char–slag transition was finished. The final slag particles (Fig. 10f) are mostly sized above 10 μm, indicating that most of the mineral matter in coal particles coalesced to form a few coarse ash particles [31–33] instead of being liberated to form lots of fine ash particles. In contrast to the coarse surface and irregular shape of the char particle (Fig. 10a–d), the coalesced ash particle has smooth surface and droplet (spherical) shape because of the surface tension of molten ash. The smooth surface and droplet shape of the ash particles suggest that the residual carbon is encapsulated by molten minerals.

On the basis of the interpretation of Fig. 10, the surface area evolution during the char–slag transition (Fig. 7) can be explained as follows. The internal surface area of a char particle is mainly created by micropores and mesopores in the particle. During the char–slag transition, a large amount of molten minerals becomes exposed on the particle surface. The melted minerals presumably have a tendency to block the macropores on the char surface, making it difficult for the adsorptive gas to diffuse into the internal structure of the particle. The more melted minerals covered the particle surface, the more pores became closed, leading to further internal surface area loss. After the char–slag transition, the remaining carbon was completely enclosed by the molten slag. This slag particle has the lowest internal surface area because of the high resistance for the adsorptive gas diffusing into the particle and the loss of microporosity.

Fig. 10d indicates that the char–slag transition of the PT8 coal started at about 91% conversion. SEM images of the char and slag samples prepared from the IL6 and PRB coals are presented in Figs. 11 and 12, respectively. The SEM images show that the char–slag transition occurred at 90% and 94% conversion for the IL6 and PRB coals, respectively.

3.5. Identification of char–slag transition

Changes in the physical properties of the char and slag particles, including density, size, internal surface area and morphology, indicate the critical conversion at which the char–slag transition occurs. The critical conversions determined on the basis of these properties are summarized in Table 3. For a single coal, different property changes indicate slightly different critical conversions, suggesting that the char–slag transition is a transitional process instead of an abrupt transformation.

In a partially converted char particle, the two main components are residual carbon and ash. When there is adequate residual carbon to encapsulate the ash, the particle behaves as a solid

char. When the ash starts encapsulating the carbon, the char–slag transition occurs and the particle is an intermediate between char and slag. When the residual carbon is encapsulated by the ash, the transition is finished and the particle transforms into molten slag. This indicates that the char–slag transition occurs when the ash content in the char particle reaches a threshold value. Data in Table 3 suggest that the critical conversion increases with decreasing ash content in the parent coal. This is because the coal with lower ash content needs a higher conversion to burn enough carbon for the included minerals to become exposed from the carbon matrix and to cover the particle surface.

4. Conclusion

The char–slag transition features dramatic changes in the physical properties of the particle. The particle density increases due to particle size reduction. The particle size reduces because of particle shrinkage in the initial stage and particle fragmentation in the later stages of the burnout process. The particle surface area decreases, which is attributed to blockage of pores in the particle by molten ash and loss of microporosity induced by carbon consumption. These physical phenomena were used to identify the critical conversion of the transition. The transition occurs at high conversions at which ash is the dominant component in the particle. Moreover, the critical conversion is dependent on the parent coal ash content at temperatures above the ash fluid temperatures. The transition takes place at lower conversion for a coal with higher ash content.

Caution needs to be exercised when interpreting the char-slag transition because it is strongly influenced by the fragmentation behavior of char particles. If fragmentation occurs in the early stage of char gasification (which does occur for highly macroporous, thin-walled char [31, 32]), large amounts of included minerals will become exposed resulting earlier transition. Char fragmentation is highly dependent on coal rank, char structure and reaction conditions. For

example, high reaction temperature may cause fragmentation compared to low reaction temperature. In addition, the critical conversions in this work were determined at temperatures above the ash fluid temperatures of the coal ashes. In certain practical coal gasifiers, coal particles are mixed with additives for achieving a slagging operation condition. The additives might affect the char–slag transition by interacting with the coal ash and lowering its ash fluid temperature.

5. Acknowledgement

This material is based upon work supported by the United States Department of Energy under Award Number FC26-08NT0005015. Matthew Delong is appreciated for training us using the SEM. Thanks also go to Dana Overacker and Scott Sinquefield for their help in designing, constructing and maintaining the LEFR.

6. Supplementary data

The ash chemistry of the three coals used in this work is presented in the supplementary data. This material is available free of charge via the Internet at http://www.elsevier.com.

7. References

1. C. Higman, M.J. Van der Burgt, Gasification, second ed., Gulf Professional Publishing, Boston, 2008.
2. S. Lin, M. Hirato, M. Horio, The characteristics of coal char gasification at around ash melting temperature, Energy Fuels 8 (1994) 598–606.
3. E.M. Hodge, D.G. Roberts, D.J. Harris, J.F. Stubington, The significance of char morphology to the analysis of high-temperature char-CO_2 reaction rates, Energy Fuels 24 (2010) 100–107.
4. T. Wu, E. Lester, M. Cloke, A burnout prediction model based around char morphology, Energy Fuels 20 (2006) 1175–1183.
5. X. Zhao, C. Zeng, Y. Mao, W. Li, Y. Peng, T. Wang, B. Eiteneer, V. Zamansky, T.F. Fletcher, The surface characteristics and reactivity of residual carbon in coal gasification slag, Energy Fuels 24 (2010) 91–94.
6. J. Gu, S. W, Y. Wu, Y. Li, J. Gao, Differences in gasification behaviors and related properties between entrained gasifier fly ash and coal char, Energy Fuels 22 (2008) 4029–4033.
7. L.E. Bool, S.A. Johnson, The effect of residual carbon on ash deposition behavior, ASME Environ. Control Div. Publ. EC, (1995) 305–312.

8. Li S, Wu Y, Whitty KJ. Ash deposition behavior during char–slag transition under simulated gasification conditions. Energy Fuels 2010; 24:1868–76.
9. C. Chen, M. Horio, T. Kojima. Numerical simulation of entrained flow coal gasifiers, part 1: modeling of coal gasification in an entrained flow gasifier, Chem. Eng. Sci. 55 (2000) 3861–3874.
10. D.F. Fletcher, B.S. Haynes, J. Chen, J.D. Joseph. Computational fluid dynamics modeling of an entrained flow biomass gasifier, Appl. Math. Model. 22 (1998) 747–757.
11. Y. Wu, J. Zhang, M. Wang, G. Yue, J. Lu, 3D numerical simulation of Texaco gasifier using assumed PDF model, Huagong Xuebao 58 (2007) 2369–2374.
12. H. Tominaga, T. Yamashita, T. Ando, N. Asahiro. Simulator development of entrained flow coal gasifiers at high temperature and high pressure atmosphere, IFRF Combust. J. No.200004 (2000)
13. X. Wang, D. Zhao, L. He, L. Jiang, Q. He, Y. Chen. Modeling of a coal-fired slagging combustor: development of a slag submodel, Combust. Flame 149 (2007) 249–260.
14. F. Montagnaro, P. Salatino, Analysis of char–slag interaction and near-wall particle segregation in entrained-flow gasification of coal, Combust. Flame 157 (2010) 874–883.
15. B. Liu, H.E. Garcia, L.L. Baxter, A simplified phase equilibrium algorithm used to predict ash/slag behaviors in slagging gasifiers/combustors, In: Annu. Int. Pittsburgh Coal Conf., PCC–Proc. Pittsburgh, September 29–October 2, 2008.
16. ASTM Standard D5142, 2009, Standard Test Methods for Proximate Analysis of the Analysis Sample of Coal and Coke by Instrumental Procedures, ASTM International, West Conshohocken, U.S., 2009, DOI: 10.1520/D5142-09, http://www.astm.org.
17. C. Tsai, A.W. Scaroni, The structural changes of bituminous coal particles during the initial stages of pulverized-coal combustion, Fuel 66 (1987) 200–206.
18. A.G. Borrego, D. Alvarez. Comparison of chars obtained under oxy-fuel and conventional pulverized coal combustion atmospheres, Energy Fuels 21 (2007) 3171–3179.
19. M.A. Field, Measurement of the effect of rank on combustion rates of pulverized coal, Combust. Flame 14 (1970) 237–248.
20. D.J. Maloney, E.R. Monazam, K.H. Casleton, C.R. Shaddix, Evaluation of char combustion models: measurement and analysis of variability in char particle size and density, Proc. Combust. Inst. 30 (2005) 2197–2204.
21. R.H. Hurt, D.R. Dudek, J.P. Longwell, A.F. Sarofim, The phenomenon of gasification-induced carbon densification and its influence on pore structure evolution, Carbon 26 (1988) 433–449.
22. R.H. Hurt, A.F. Sarofim, J.P. Longwell, Gasification-induced densification of carbons: from soot to form coke, Combust. Flame 95 (1993) 430–432.
23. E. Bar-Ziv, I.I. Kantorovich, Mutual effects of porosity and reactivity in char oxidation, Prog. Energy Combust. Sci. 27 (2001) 667–697.
24. I.I. Kantorovich, E. Bar-Ziv. Processes in highly porous chars under kinetically controlled conditions: I. evolution of the porous structure, Combust. Flame 97 (1994) 61–78.
25. L.L. Baxter, Char fragmentation and fly ash formation during pulverized-coal combustion, Combust. Flame 90 (1992) 174–184.
26. E. Bar-Ziv, I.I. Kantorovich, Mutual Effects of Porosity and Reactivity in Char Oxidation, Prog. Energy Combust. Sci. 27 (2001) 667–697.

27. H. Liu, C. Luo, S. Kato, S. Uemiya, M. Kaneko, T. Kojima. Kinetics of CO_2/char gasification at elevated temperatures, part I: experimental results. Fuel Process. Technol. 87 (2006) 775–781.
28. R.P. Gupta, T.F. Wall, I. Kajigaya, S. Miyamae, Y. Tsumita. Computer-controlled scanning electron microscopy of minerals in coal–implications for ash deposition, Prog. Energy Combust. Sci. 24 (1998) 523–543.
29. Y. Liu, R.P. Gupta, A. Sharma, T. Wall, A. Butcher, G. Miller, P. Gottlieb, D. French, Mineral matter–organic matter association characterization by QEMSCAN and applications in coal utilization, Fuel 84 (2005) 1259–1267.
30. A.F. Sarofim, J.B. Howard, A.S. Padia, Physical transformation of the mineral matter in pulverized coal under simulated combustion conditions, Combust. Sci. Technol. 16 (1977) 187–204.
31. H. Wu, T. Wall, G. Liu, G. Bryant, Ash liberation from included minerals during combustion of pulverized coal: the relationship with char structure and burnout, Energy Fuels 13 (1999) 1197–1202.
32. S.G. Kang, A.F. Sarofim, J.M. Beér, Effect of char structure on residual ash formation during pulverized coal combustion, In: Proceedings of the 24th International Symposium on Combustion. Sydney, England, July 5–10, 1992; p. 1153–59.
33. S.A. Benson, E.A. Sondreal, P.J. Hurley, Status of coal ash behavior research, Fuel Process. Technol. 44 (1995) 1–12.

8. Figures

Fig. 1. Schematic diagram of the LEFR used for preparing char and ash particles.

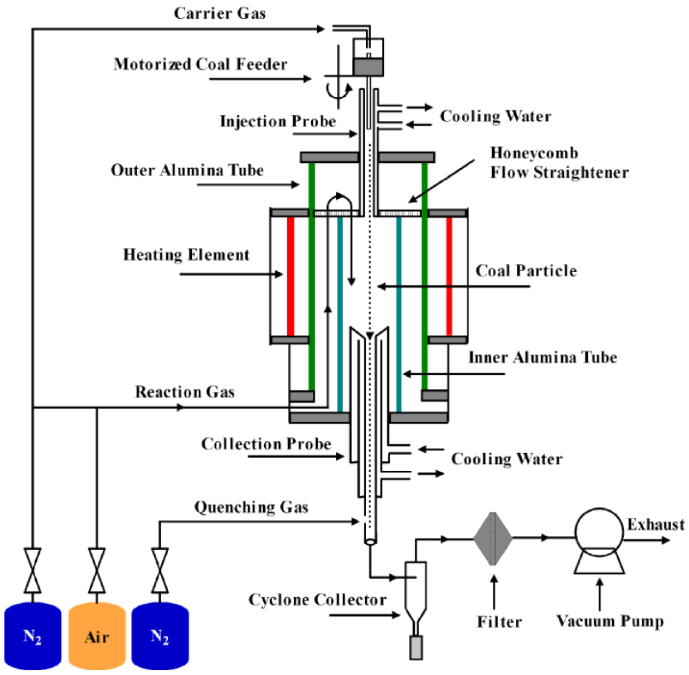

Fig. 2. Burnout behavior of the PT8, IL6 and PRB coals. The data of IL6 were adapted from Li and Whitty [20].

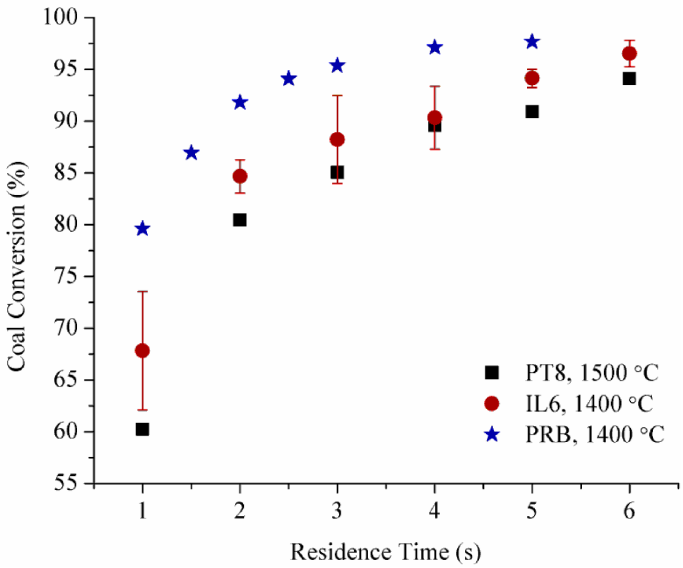

Fig. 3. Particle densities of the char and slag particles prepared from the PT8 coal.

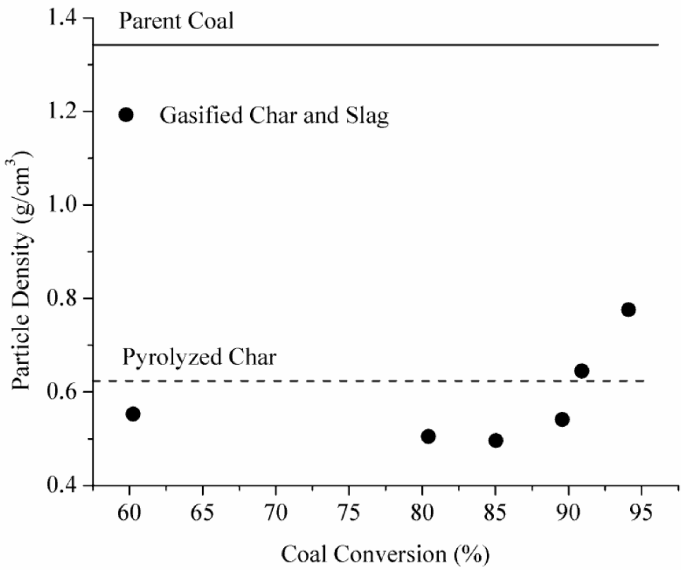

Fig. 4. Particle sizes of the char and slag particles prepared from the PT8 coal determined with two methods.

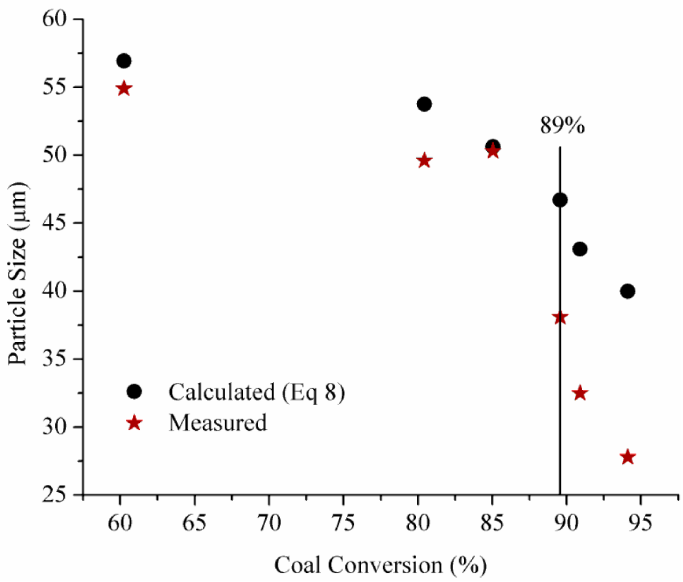

Fig. 5. Particle densities of the char and slag particles prepared from the IL6 and PRB coals.

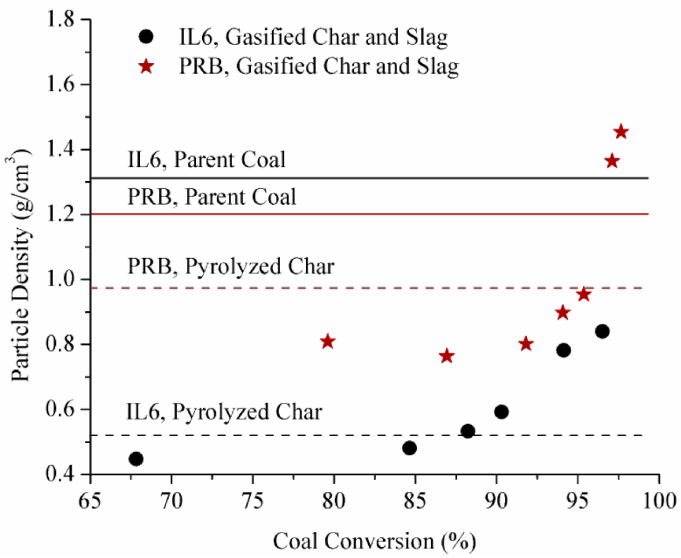

Fig. 6. Particle sizes of the char and slag particles prepared from the IL6 and PRB coals.

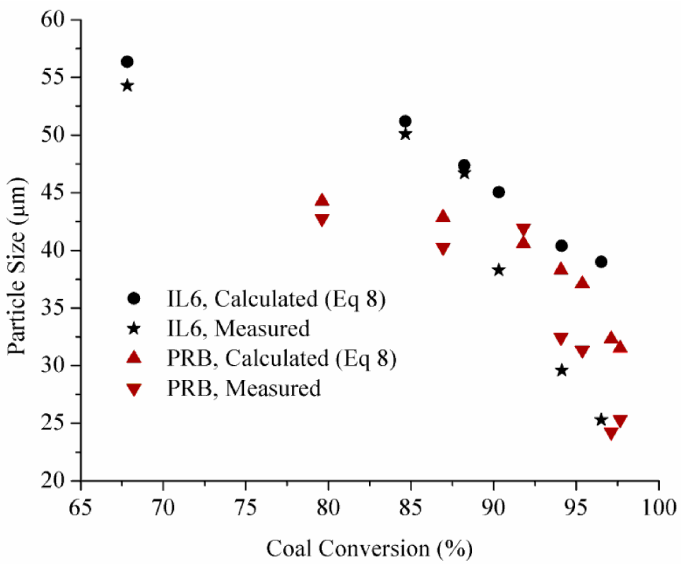

Fig. 7. Total and micropore surface areas of the char and slag particles prepared from the PT8 coal.

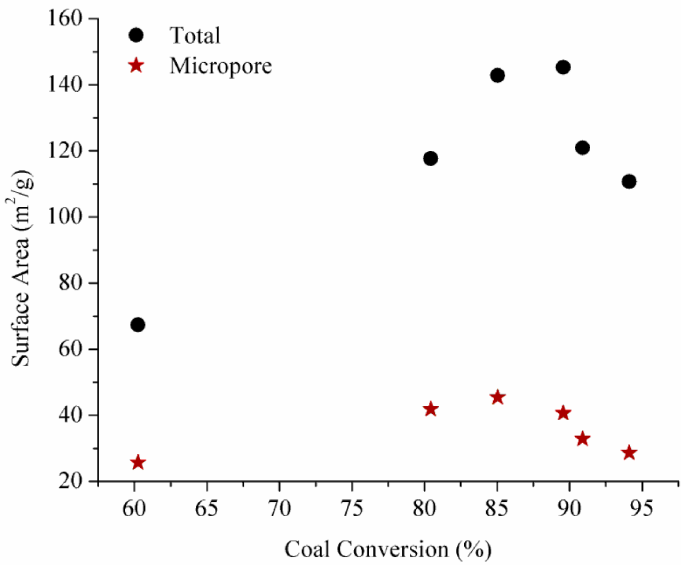

Fig. 8. Total and micropore surface areas of the char and slag particles prepared from the IL6 coal. The total surface area data were adapted from Li and Whitty [20].

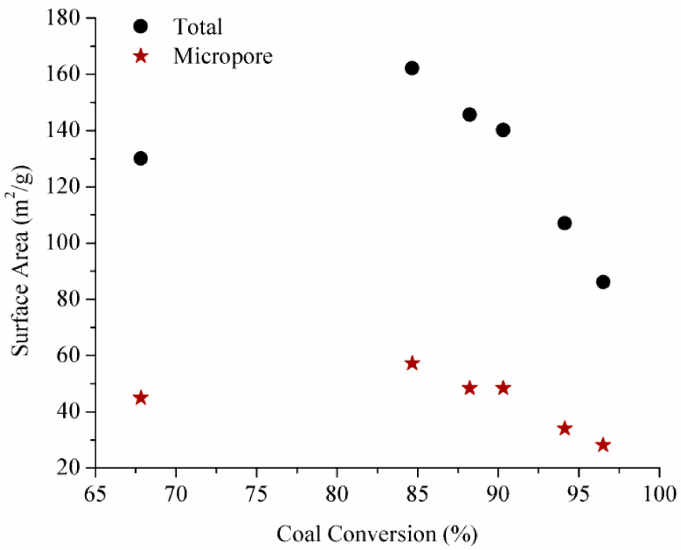

Fig. 9. Total and micropore surface areas of the char and slag particles prepared from the PRB coal.

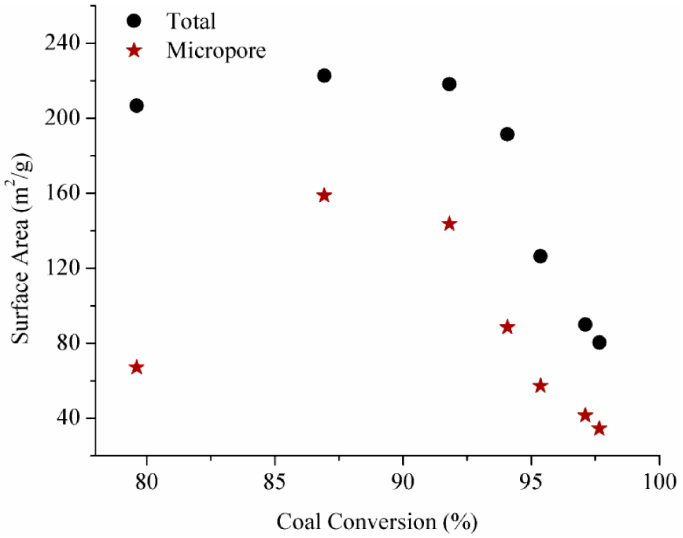

Fig. 10. SEM images of the char and slag particles prepared from the PT8 coal.

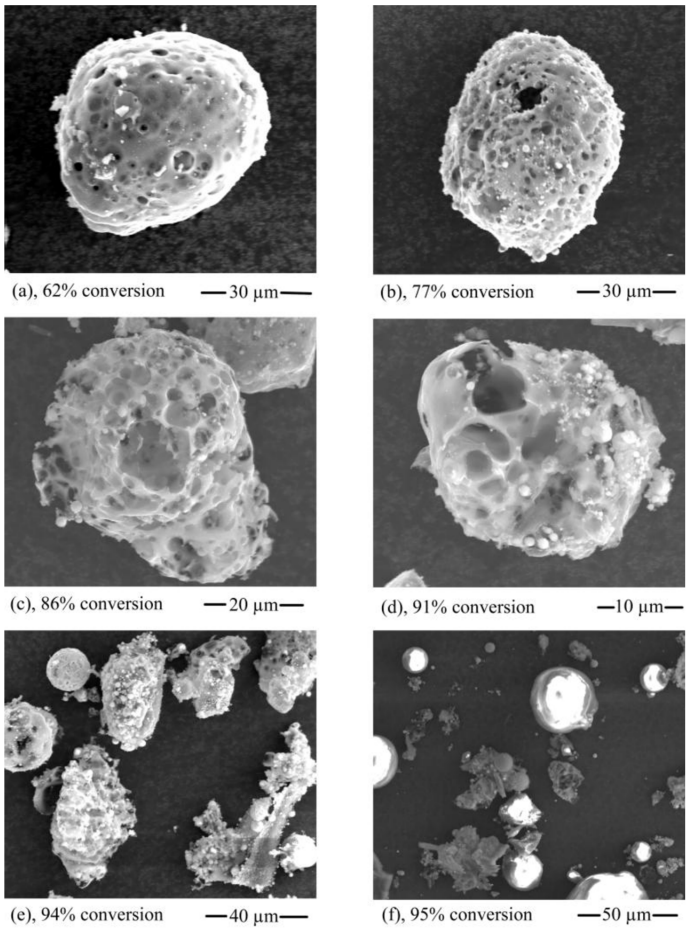

Fig. 11. SEM images of the char and slag particles prepared from the IL6 coal. Images a–d were adapted from Li and Whitty [20].

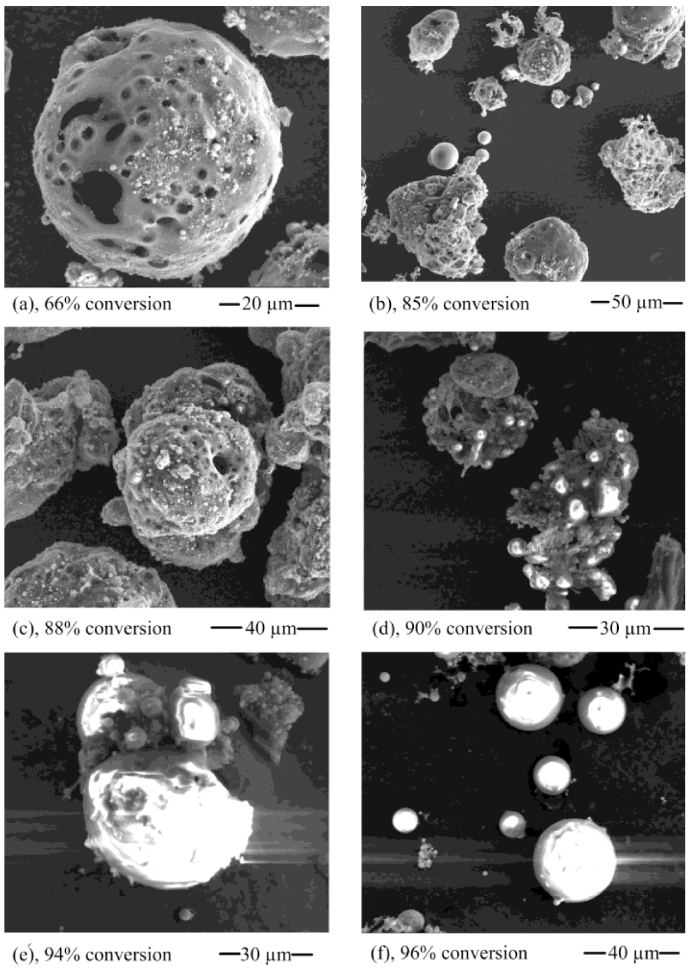

Fig. 12. SEM images of the char and slag particles prepared from the PRB coal.

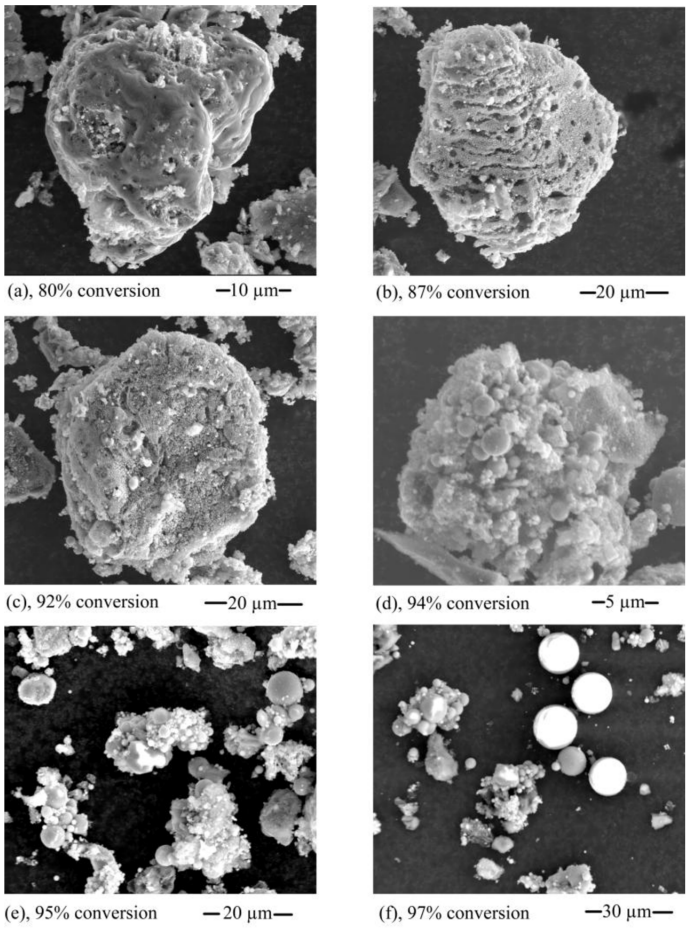

Tables

Table 1. Proximate and ultimate analyses of the coals used in this work.

Coal	Proximate Analysis (wt%, mf)[a]				Ultimate Analysis (wt%, maf)[b]				
	Moisture[c]	Ash	Volatiles	Fixed Carbon	C	H	N	S	O
PT8	1.08	9.00	38.22	52.64	84.07	5.58	1.53	3.86	4.96
IL6	3.63	10.89	36.42	52.69	74.52	4.96	1.48	4.66	14.38
PRB	24.59	6.82	49.07	44.11	77.91	3.63	1.18	0.35	16.93

[a]Moisture free, method: ASTM D5142. [b]Moisture ash free, method: ASTM D5142/5373. [c]As received.

Table 2. Ash fusion temperatures of the coals used in this work.

Coal	Ash Fusion Temperature (reducing, °C)[a]			
	IT	ST	HT	FT
PT8	1085	1104	1137	1229
IL6	1104	1116	1139	1246
PRB	1142	1150	1160	1191

[a]Method: ASTM D1857.

UU IR Author Manuscript

Table 3. Critical conversions of the char–slag transition for different coals determined from different properties.

Coal	Critical Conversion (%)					
	Particle Density	Particle Size	Surface Area	Morphology	Confident	Median
PT8	89	89	91	91	89–91	90
IL6	88	90	88	90	88–90	89
PRB	92	94	92	94	92–94	93